J Appl Physiol 92: 2381–2389, 2002.
First published February 22, 2002; 10.1152/japplphysiol.00843.2001.

Nonuniform shortening in the biceps brachii during elbow flexion

GEORGE P. PAPPAS,[1,2,3] DEANNA S. ASAKAWA,[1,2,3] SCOTT L. DELP,[3,4] FELIX E. ZAJAC,[1,3,4] AND JOHN E. DRACE[2]
[1]*Rehabilitation Research and Development Center and* [2]*Diagnostic Radiology Center, Veterans Affairs Palo Alto Health Care System, Palo Alto 94304; and Departments of* [3]*Mechanical Engineering (Biomechanical Engineering Division) and* [4]*Functional Restoration, Stanford University, Stanford, California 94305*

Received 10 August 2001; accepted in final form 13 February 2002

Pappas, George P., Deanna S. Asakawa, Scott L. Delp, Felix E. Zajac, and John E Drace. Nonuniform shortening in the biceps brachii during elbow flexion. *J Appl Physiol* 92: 2381–2389, 2002. First published February 22, 2002; 10.1152/japplphysiol.00843.2001.—This study tested the common assumption that skeletal muscle shortens uniformly in the direction of its fascicles during low-load contraction. Cine phase contrast magnetic resonance imaging was used to characterize shortening of the biceps brachii muscle in 12 subjects during repeated elbow flexion against 5 and 15% maximum voluntary contraction (MVC) loads. Mean shortening was relatively constant along the anterior boundary of the muscle and averaged 21% for both loading conditions. In contrast, mean shortening was nonuniform along the centerline of the muscle during active elbow flexion. Centerline shortening in the distal region of the biceps brachii (7.3% for 5% MVC and 3.7% for 15% MVC) was significantly less ($P < 0.001$) than shortening in the muscle midportion (26.3% for 5% MVC and 28.2% for 15% MVC). Nonuniform shortening along the centerline was likely due to the presence of an internal aponeurosis that spanned the distal third of the longitudinal axis of the biceps brachii. However, muscle shortening was also nonuniform proximal to the centerline aponeurosis. Because muscle fascicles follow the anterior contour and centerline of the biceps brachii, our results suggest that shortening is uniform along anterior muscle fascicles and nonuniform along centerline fascicles.

skeletal muscle; contraction; heterogeneity; upper limb; magnetic resonance imaging

MECHANICAL MODELS OF MUSCLE contraction often assume that skeletal muscle fibers shorten uniformly (22, 44). However, uniform shortening of muscle fibers may not exist in biological reality because whole muscle is a composite of contractile and connective tissue (21, 31). It has been suggested that the complexity of muscle architecture and the heterogeneity in the mechanical properties of muscle and tendon tissue may lead to inhomogeneous shortening (11, 27, 39, 46). Nonuniform shortening has important functional consequences. For example, length nonuniformity at the level of the sarcomere, myofiber, or fascicle can alter the force-length properties of whole muscle and introduce inaccuracy in the estimation of muscle force (18, 20, 32).

In vivo measurements of contracting human muscle are needed to test the validity of biomechanical modeling assumptions, improve the accuracy of representations of muscle-tendon mechanics, and further the understanding of musculoskeletal function. Cine phase contrast magnetic resonance imaging (cine PC MRI) has been used to measure the motion of muscle, tendon, and trabecular bone accurately and noninvasively (7, 8, 38). Previous studies have demonstrated that cine PC MRI tracks skeletal muscle with a root mean square error of 1 mm (9) and trabecular bone with an average absolute error of <0.7 mm (38). Noninvasive imaging modalities, such as MRI and ultrasound imaging, have been used to characterize in vivo skeletal muscle architecture (13, 34). Knowledge of in vivo muscle architecture provides important information that enables the interpretation of cine PC MRI motion data and the characterization of muscle contraction mechanics in humans.

The goal of this study was to examine the uniformity of shortening in the human biceps brachii muscle-tendon complex. The biceps brachii complex, which includes the long and short head muscles, is fusiform in shape, with muscle fibers inserting at an angle into tendons at each end (Fig. 1). The distal biceps tendon flattens into a straplike internal aponeurosis, whereas the proximal tendons form external aponeuroses. The internal aponeurosis is located along the distal centerline of the muscle and spans 34% of the length of biceps brachii long head muscle (L_M) (36).

Muscle shortening was measured within the biceps brachii during active elbow flexion against 5 and 15% of maximum voluntary contraction (MVC) strength. We hypothesized that shortening would be uniform along the fascicle direction in regions of the muscle that do not contain aponeurosis tissue and nonuniform

Address for reprint requests and other correspondence: G. P. Pappas, Diagnostic Radiology Center (114), VA Palo Alto Health Care System, 3801 Miranda Ave., Palo Alto, CA 94304 (E-mail: gpappas@stanford.edu).

The costs of publication of this article were defrayed in part by the payment of page charges. The article must therefore be hereby marked "*advertisement*" in accordance with 18 U.S.C. Section 1734 solely to indicate this fact.

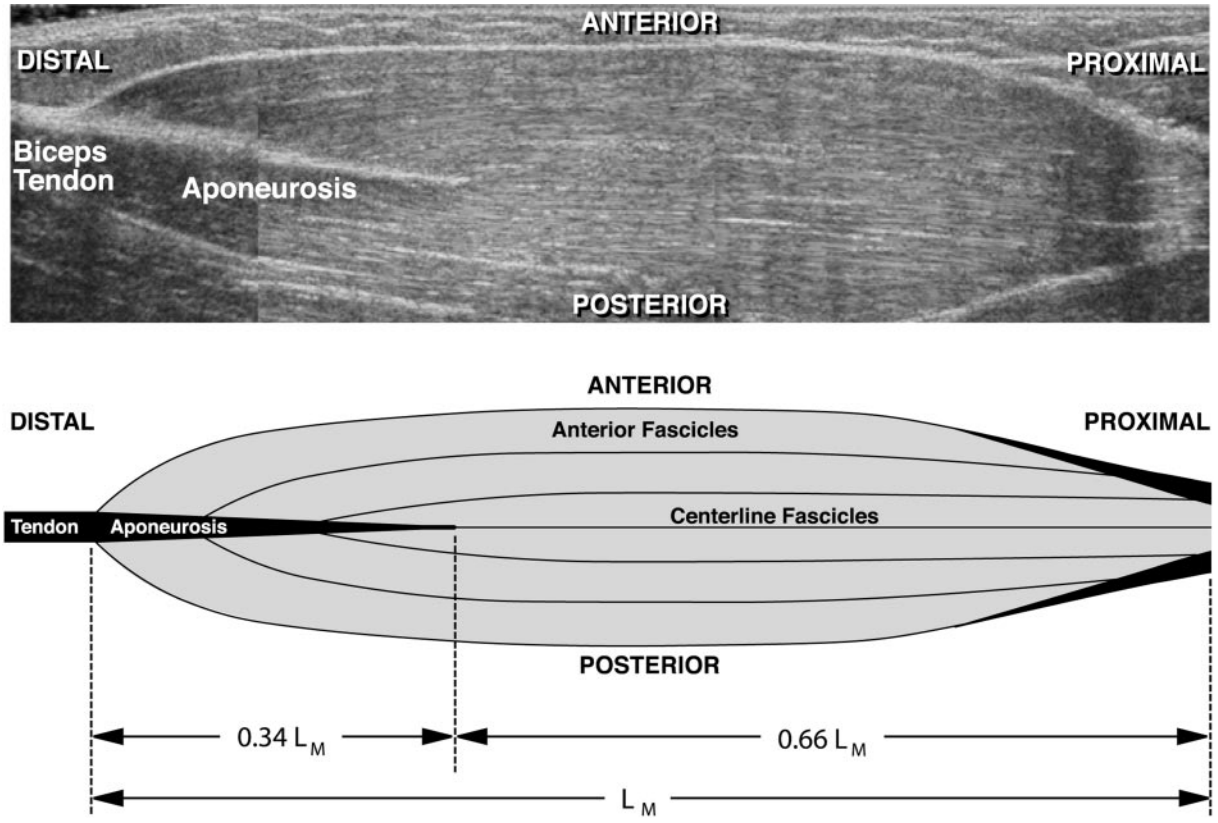

Fig. 1. Composite ultrasound image (*top*) and schematic line drawing (*bottom*) of biceps brachii architecture as viewed in sagittal plane. Insertion of muscle fascicles along the distal internal aponeurosis and proximal external aponeuroses results in individual fascicles that are shorter than the length of the muscle [long head muscle length (L_M)]. Internal aponeurosis spans 34% L_M and implies that centerline muscle fascicle length is 66% L_M. Fascicles of the biceps brachii are expected to be of uniform length (5).

in regions that contain aponeurosis tissue. On the basis of the specific architecture of the biceps brachii, we hypothesized that shortening would be uniform along the anterior boundary and proximal centerline of the biceps brachii and nonuniform along the distal centerline in the region containing the internal aponeurosis (Fig. 1). This study tests these hypotheses and provides the first in vivo measurements of muscle shortening uniformity along the fascicle direction in human subjects.

METHODS

Twelve unimpaired subjects (10 men and 2 women, age 21–44 yr, height 160–188 cm) volunteered for participation in this study. Average anthropometric characteristics of the subjects are presented in Table 1. Each subject performed three cyclic elbow flexion tasks within a 1.5-T General Electric MR scanner (Signa, General Electric Medical Systems, Milwaukee, WI). Before MR imaging, the muscle fascicle architecture of the biceps brachii was measured in each subject by using ultrasound imaging with the elbow extended and flexed 90° (36). An Acuson Sequoia 512 ultrasound system (Mountain View, CA) with a 15-MHz transducer was used to image the midsagittal plane of the biceps brachii (Fig. 1, *top*). The Institutional Review Board at Stanford University approved the protocol, and informed consent was obtained from each subject.

Each subject was positioned on their side on the MRI scanner table next to a plastic exercise device that was attached to the table (Fig. 2). The subject's right hand was placed in a glove and fastened to the handle of the device in ~60° of forearm supination to ensure activation of the biceps brachii (6). The exercise device was designed to guide the elbow flexion and extension motion and to ensure the subject's upper arm remained stationary during data acquisition. The range of motion of elbow flexion was ~80°; elbow angle was measured with a goniometer as 7 ± 5° at maximum extension and 86 ± 5° at maximum flexion.

Table 1. *Age and anthropometric characteristics of the subjects*

Measurement	Means ± SD
Age, yr	30 ± 7
Height, cm	181.9 ± 11.6
Weight, kg	72.9 ± 6.9
MVC, kg	21.7 ± 4.4
Upper arm length, cm	32.9 ± 1.6
Upper arm circumference, cm	32.6 ± 2.6

Values are for 12 subjects. MVC, maximum voluntary contraction load with 90° elbow flexion. Upper arm length was measured from the lateral edge of the acromion to lateral humeral epicondyle. Arm circumference was measured as the maximum with the elbow flexed 90° in weak isometric contraction.

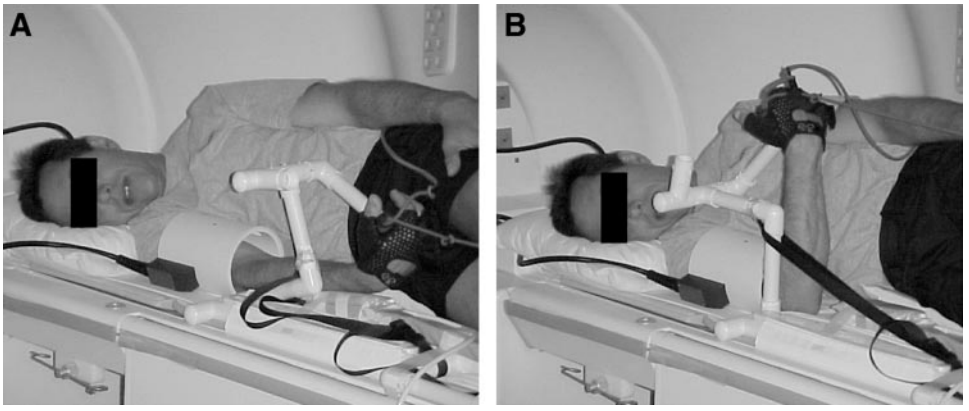

Fig. 2. Subject positioned on the magnetic resonance scanning table with the elbow flexion exercise device before magnetic resonance imaging. *A*: center of rotation of the subject's elbow, approximated by the lateral humeral condyle, was aligned with the rotational axis of the device. Two different-sized devices were constructed to accommodate the variable forearm length of the subjects. Two calibrated elastic cords attached to the device provided the desired elbow flexion load. *B*: an adjustable nylon band limited elbow flexion to a maximum of 90° and prevented contact of the forearm with the cylindrical radio-frequency data acquisition coil surrounding the upper arm.

Static MR images were acquired to ensure that the longitudinal axes of the biceps brachii and humerus were oriented parallel to the longitudinal axis of the scanner. Once aligned, the subject was instructed to keep his or her upper arm in the same position for the duration of the experiment. Before three successive dynamic cine PC MRI data acquisitions, static axial MR images were acquired with the elbow in the extended position and in the maximum flexion position while the subjects were resisting 5% MVC. After the dynamic cine PC MRI scans, a final series of static axial images was acquired to confirm the upper arm had remained stationary during the cine PC data acquisitions; the medial-lateral and anterior-posterior position of the humerus in the post-cine PC axial MR images was compared with its initial position in the pre-cine PC axial images. Static images were acquired at 10-mm intervals along the upper arm by using a proton density, fast spin-echo sequence with fat saturation, 12 × 12-cm field of view, 256 × 160 pixel matrix, and 7-mm slice thickness. The position of the distal aponeurosis and the boundaries of the long and short heads of the biceps were determined from these static images.

Cine PC MRI was used to measure muscle tissue motion within the biceps brachii noninvasively during repeated elbow flexion. Cine PC data were acquired from the upper arm under three different loading conditions: passive elbow flexion and active elbow flexion against 5 and 15% of the subject's elbow flexion MVC strength. The MVC strength of each subject was measured before imaging from the average of three maximal isometric efforts at an elbow angle of 90°. The three elbow flexion tasks were performed in a randomized order. The 15% MVC force condition was considered to be the maximum resistance that would not cause substantial fatigue (14, 30). As a baseline reference, biceps motion was also measured during passive flexion and extension of the elbow; each subject was instructed to keep their arm completely relaxed while their elbow was flexed and extended by the investigator using a rod attached to the exercise device. Absence of biceps brachii activity during the passive elbow flexion task was confirmed in three subjects by surface electromyography measurements made outside the MRI scanner. Each cyclic elbow flexion task was performed at a rate of 35 cycles/min (to the beat of a metronome) for ~2 min. Sixty-four repetitions were needed to acquire 64 lines of data in the frequency domain (37); several additional repetitions were required for the subject to attain a repeatable motion before the initiation of data collection. Data collection was synchronized to the motion cycle by using an optical transducer, triggered at full extension, and data were interpolated to 24 time frames. Cine PC MR images (1 magnitude image and 3 velocity images per time frame) were acquired by using a 17-ms repetition time, 30° flip angle, 35 cm/s maximum encoding velocity, 28 × 14-cm field of view, 256 × 128 pixel matrix, and 10-mm slice thickness. The cine PC imaging plane was prescribed graphically with an oblique-sagittal orientation by using the static axial images of the upper arm flexed against a 5% MVC load (Fig. 3).

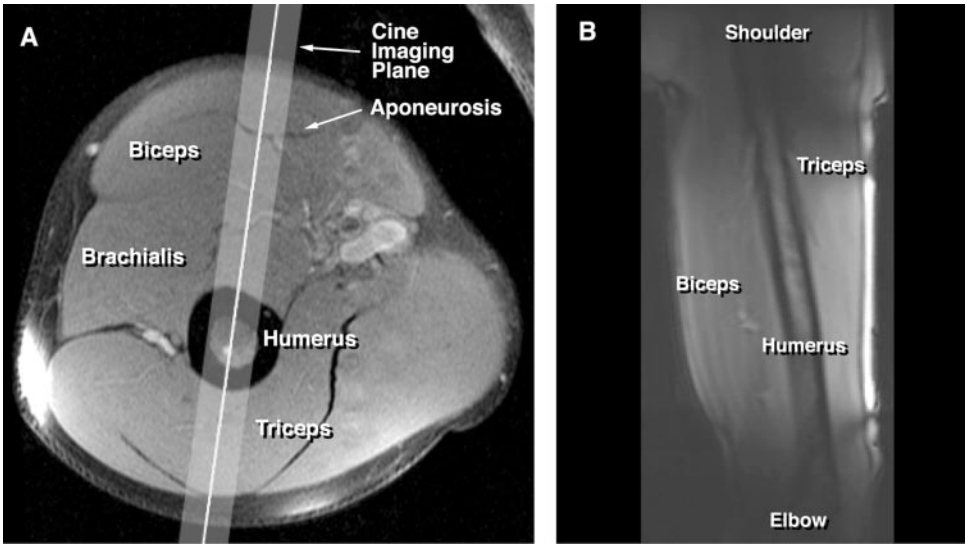

Fig. 3. Representative static axial and cine phase contrast magnitude images. *A*: graphic prescription of the oblique-sagittal cine phase contrast imaging plane on a static axial image of the arm. Imaging plane was aligned with the longitudinal axis of the biceps (and therefore the muscle fascicle direction) to minimize out-of-plane tissue motion. The imaging plane also bisected the distal aponeurosis and biceps brachii muscle belly, and it intersected the humerus. *B*: resulting cine phase contrast magnitude image in the oblique-sagittal imaging plane during *time frame 1*, with the elbow fully extended.

Shortening in the biceps brachii was determined by tracking the position of muscle tissue regions of interest (ROIs) over all 24 time frames of the motion cycle, which included both flexion and extension of the elbow. All ROIs were 1-cm^2 square regions and were prescribed graphically in the first magnitude image (*time frame 1*) when the elbow was maximally extended (Fig. 4). Three-dimensional displacement trajectories were computed for each ROI from the three orthogonal sets of velocity images by using a closed-form Fourier integration method (45).

Percent shortening was measured along the anterior boundary and centerline of the biceps brachii by comparing the positions of tissue regions at maximum elbow flexion to their initial positions at maximum elbow extension. Normalized length change was defined as $(L_F - L_E)/L_E$, where L_E and L_F were the distances between two ROIs at maximum elbow extension and flexion, respectively. Percent length change was computed between every second region, ROI_n and ROI_{n+2}. Because the 1 × 1-cm ROIs were defined in a contiguous distribution along the muscle in the first magnitude image (with the elbow fully extended), L_E was ~2 cm. A negative length change indicated local muscle shortening during elbow flexion.

Shortening along the anterior border of the biceps was determined from the position trajectories of the ROIs located along the anterior boundary of the muscle, just deeper than the subcutaneous fat layer (Fig. 4*A*). Because anterior fascicles follow the contour of the anterior boundary of the biceps brachii (Fig. 1), shortening along the direction of anterior fascicles could be measured by tracking anterior ROIs. Centerline shortening was determined from the position trajectories of ROIs along the longitudinal axis of the biceps brachii (Fig. 4*B*). The most distal centerline ROI was defined ~1–2 cm proximal to the distal biceps tendon, as permitted by the subject's muscle thickness and shape. Distal aponeurosis length was 7 ± 1 cm and L_M was 20 ± 2 cm for the 12 subjects (36). Because the distal aponeurosis spanned an average of 34% of the muscle's longitudinal length, centerline ROIs defined over the distal third of the muscle contained aponeurosis tissue. By using the measured aponeurosis length for each subject, centerline shortening data were subdivided into two regions: *1*) the distal aponeurosis-containing region (i.e., intra-aponeurosis region) and *2*) the proximal region that did not contain aponeurosis (i.e., extra-aponeurosis region).

Percent shortening was computed as a function of normalized distance from the distal biceps tendon; normalization was based on L_M. For each subject, the values of percent shortening were linearly interpolated to increments of 2.5% of L_M. The distributions of mean anterior and centerline shortening were compared at each location along the muscle by using two-sided, paired *t*-tests. To test for uniform shortening, 95% confidence intervals for average shortening at each location along the muscle (in 2.5% length increments) were compared with the overall mean of the shortening distribution. A linear regression analysis was also performed to compare the slopes of the anterior and centerline shortening distributions, with separate regression slopes computed for intra-aponeurosis and extra-aponeurosis centerline shortening. Data from all 12 subjects were used to analyze centerline shortening. However, because of inadequate muscle thickness in one subject, the analysis of anterior shortening was based on 11 subject data sets. Descriptive statistics are reported as means ± SD.

RESULTS

Shortening along the anterior boundary of the biceps brachii was relatively uniform during active elbow flexion (Fig. 5*A*). Mean anterior shortening did not differ significantly between the 5 and 15% MVC loading conditions; the overall average of the mean anterior shortening distribution was 21% for both the 5 and 15% MVC loading conditions. For the 5% MVC condition, the 21% overall mean value of anterior shortening was within the 95% confidence level for 22 of the 24

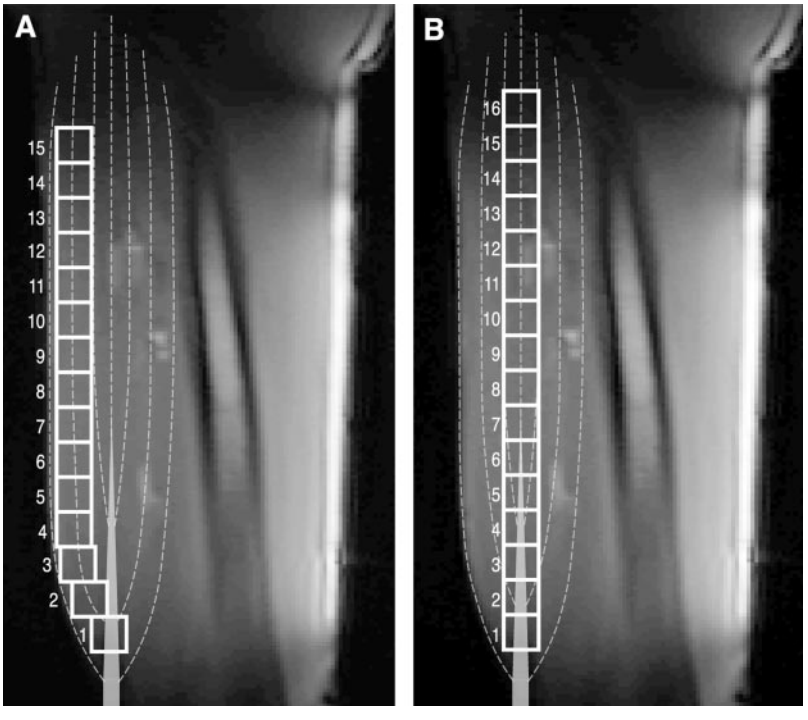

Fig. 4. Prescription of tissue regions of interest in the first cine magnitude image of the cycle (*time frame 1*) with the elbow fully extended. Each prescribed distribution contains 12–16 contiguous 1-cm^2 regions of interest, as permitted by the subject's muscle length and shape and the magnetic resonance signal strength at the proximal end of the muscle. A depiction of the internal aponeurosis (solid gray area) and muscle fascicle orientation (dashed gray lines) is superimposed on the image to orient the reader. *A*: regions of interest prescribed along the anterior border of the biceps brachii in the first cine magnitude image. Care was taken to ensure that regions of interest did not encompass any subcutaneous fat during any of the time frames. *B*: distribution of centerline regions of interest along the longitudinal axis of biceps brachii for the same subject. Longitudinal axis of the biceps brachii was defined by using the spatial coordinates of the distal biceps tendon and the centroid of the biceps in a proximal location as determined from static anatomic images.

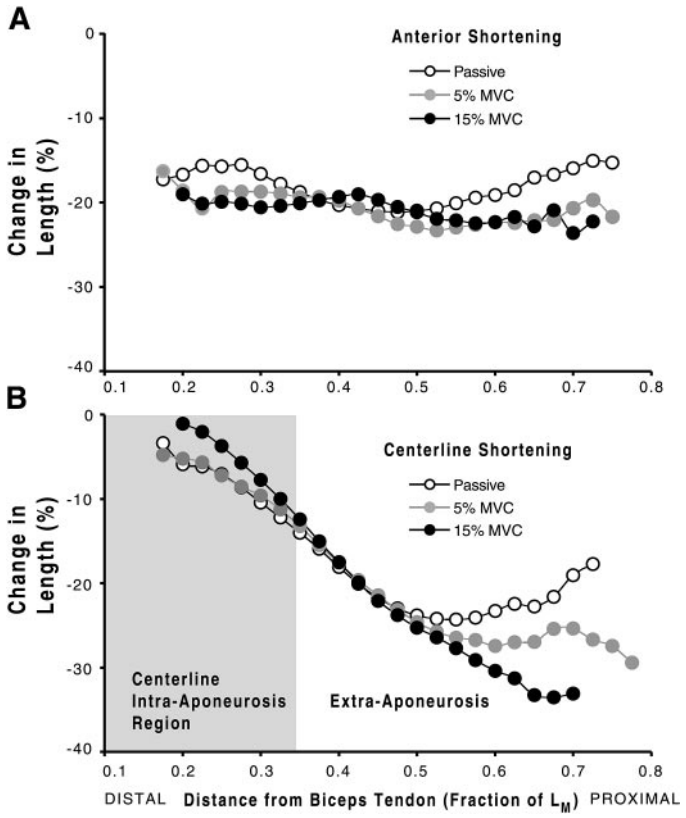

Fig. 5. Mean shortening along the biceps brachii during maximum elbow flexion against 5 and 15% maximal voluntary contraction (MVC) and during passive flexion of the elbow. Percent shortening is plotted as a function of distance from the distal tendon, normalized by the length of the biceps brachii long head muscle belly. Negative values of % length change indicate muscle shortening with elbow flexion. *A*: mean shortening along the anterior boundary of the biceps brachii. *B*: mean shortening along the centerline of the biceps is nonuniform.

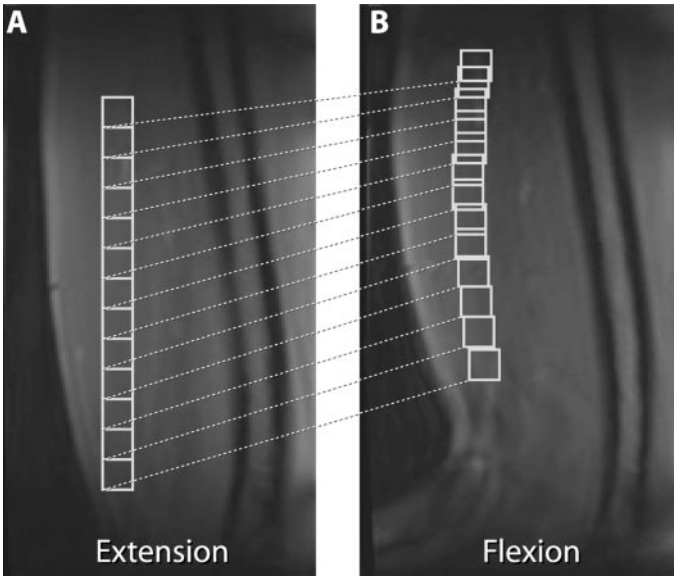

Fig. 6. Nonuniform displacement of tissue regions along the centerline of the biceps brachii during flexion and extension of the elbow (5% MVC force condition). Centerline regions of interest are graphically displayed on the corresponding cine magnitude images. Dashed lines have been added for visualizing the relative positions of the tissue regions of interest during the motion cycle. *A*: regions of interest prescribed graphically along the centerline during full extension of the elbow (*time frame 1*). *B*: position of tracked centerline regions of interest at maximal elbow flexion (*time frame 11*). Greater shortening is observed along the proximal regions of the centerline compared with the distal end.

individual values of mean shortening along the muscle length. Similarly, for the 15% MVC condition, 21 of the 22 confidence intervals contained the mean of 21%. In contrast, shortening along the anterior boundary was not uniform during passive flexion of the elbow (Fig. 5*A*). Less shortening occurred at the distal and proximal ends of the muscle under the passive motion condition; only 18 of the 24 confidence intervals for mean shortening contained the distribution mean of 18% shortening.

Shortening along the centerline of the biceps brachii muscle-tendon complex was nonuniform (Figs. 5*B* and 6). For both active loading conditions (5 and 15% MVC), mean centerline shortening was significantly lower in magnitude at the distal end of the muscle, which contains aponeurosis tissue, compared with shortening at the midportion of the muscle. Mean centerline shortening averaged <5% at the distal centerline of the biceps brachii (~0.15 L_M) and increased to between 20 and 35% shortening in the midportion (0.4–0.7 L_M). Mean centerline shortening was significantly lower ($P < 0.001$) at the distal end of the biceps brachii compared with shortening in the midportion under both the 5 and 15% MVC loading conditions (Table 2). Centerline shortening was also nonuniform during passive elbow flexion (Fig. 5*B*).

Centerline shortening was nonuniform in both the intra- and extra-aponeurosis regions. Mean centerline shortening within the distal intra-aponeurosis region was found to be nonuniform and varied approximately linearly for all three loading conditions ($r = 0.975$, 0.991, and 0.981 for passive, 5% MVC, and 15% MVC, respectively). In the intra-aponeurosis region (<0.34 L_M), the linear regression slopes of centerline shortening did not differ significantly among the three different loading conditions ($P = 0.85$, 0.43, and 0.54 for passive vs. 5% MVC, passive vs. 15% MVC, and 5% vs. 15% MVC, respectively). Surprisingly, in both the 5 and 15% MVC loading cases, mean centerline shortening remained nonuniform even in the midportion and proximal regions of the muscle (>0.34 L_M), where no aponeurosis was present. The extra-aponeurosis linear

Table 2. *Comparison of centerline shortening at the distal end and midportion of the biceps brachii for active elbow flexion against 5 and 15% MVC*

	Distance From Biceps Tendon	
Loading	20% L_M	50% L_M
5% MVC	7.3 ± 5.3	26.3 ± 6.3
15% MVC	3.7 ± 4.3	28.2 ± 6.1

Values are means ± SD given in %. Shortening was compared at distances of 20 and 50% of the long head muscle length (L_M) from the biceps tendon.

regression slopes were significantly different from zero for both the 5% MVC ($P < 0.01$) and 15% MVC ($P < 0.001$) loading conditions. Moreover, the extra-aponeurosis slope was significantly greater ($P = 0.001$) for elbow flexion against 15% MVC compared with 5% MVC.

The distribution of mean anterior shortening (Fig. 5*A*) was significantly different from the distribution of mean centerline shortening (Fig. 5*B*) for active elbow flexion ($P < 0.001$). The differences in anterior and centerline shortening distributions were statistically significant for both active flexion conditions (5 and 15% MVC), with larger differences observed under the 15% MVC loading condition (Fig. 7). The intra-aponeurosis and extra-aponeurosis linear regression slopes of the centerline shortening distribution were both significantly greater ($P < 0.05$) than the slope of the anterior shortening distribution for the 5% MVC loading condition. Even larger differences ($P < 0.01$) were measured between the slopes of the centerline and anterior shortening distributions for 15% MVC loading.

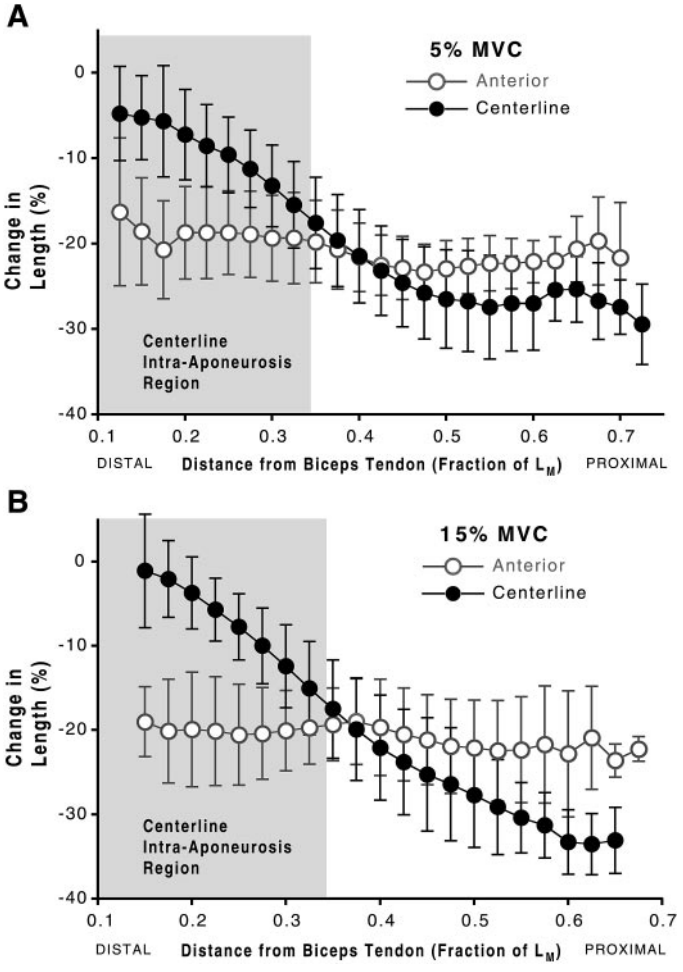

Fig. 7. Comparison of centerline and anterior shortening for 5 and 15% MVC. Distribution of mean length change along the centerline and anterior fascicles of the biceps brachii at maximum elbow flexion (86 ± 5°) against 5% MVC (*A*) and 15% MVC (*B*). Negative length changes indicate muscle shortening with elbow flexion. Error bars indicate ±1 SD of the 12 centerline shortening and 11 anterior shortening data sets.

For all cine PC MRI scans, the 12 subjects maintained the position of their upper arm within ±5 mm of its original anterior-posterior location and medial-lateral location. Maximum out-of-plane tissue motion was 10 times smaller than maximum in-plane motion, ensuring accuracy in the tracking of tissue motion (38). The maximum out-of-plane displacement for all anterior and centerline ROIs averaged over all subjects was only 2.7 ± 2.0 mm, well under the 10-mm thickness of the imaging plane. None of the subjects reported fatigue during the 5% MVC elbow flexion task; however, most subjects experienced mild fatigue at the end of the 15% MVC task.

DISCUSSION

Shortening along the anterior boundary of the biceps brachii was significantly different than shortening along the centerline during low-load (5 and 15% MVC) elbow flexion. Shortening along the anterior boundary was approximately uniform, which supports the hypothesis that anterior muscle fascicles shorten uniformly during active contraction. In contrast, nonuniform shortening was measured along the centerline of the biceps brachii. Centerline shortening was nonuniform both in the distal region of the muscle-tendon complex that contains an internal aponeurosis and in the regions of the muscle that are proximal to the internal aponeurosis. These results suggest that the internal aponeurosis, which spans the distal third of the biceps brachii, influences shortening along the entire length of centerline fascicles during elbow flexion.

Shortening was estimated along muscle fascicles based on the measured displacement of regions of muscle tissue. A possible limitation of this study was the inability to confirm the orientation of muscle fascicles during elbow flexion. However, we believe anterior and centerline shortening closely approximated fascicle shortening for the following reasons. First, ROIs were defined along the direction of muscle fascicles as determined from ultrasound images. For example, the uniform anterior shortening measured during active contraction suggests uniform shortening along anterior fascicles because these fascicles follow the contour of the anterior boundary of the muscle (Fig. 1). Moreover, the cine PC imaging plane was aligned with the longitudinal axis of the biceps brachii (Fig. 3) and should have contained anterior muscle fascicles, in addition to centerline fascicles that are parallel to the longitudinal axis (Fig. 1). Finally, the observation that in-plane displacement of tissue regions was ~10 times greater than out-of-plane displacement suggests that anterior and centerline fascicles were contained within the imaging plane.

Muscle fascicle shortening could not be accurately determined in the distal region of the biceps brachii as a result of the presence of tendinous aponeurosis tissue. Although the 1-cm^2 ROIs along the distal centerline contained both myofibrillar and tendinous tissue (Fig. 4*B*), the cine PC MR signal measured from these regions was due predominantly to myofibrillar tissue.

This is a consequence of the more rapid decay of the MR signal from tendinous tissue compared with myofibrillar tissue. Furthermore, firm conclusions about shortening along a muscle fascicle in the distal aponeurosis-containing region could not be drawn because of the complex interaction between muscle fascicles and aponeurosis and because of the insertion of muscle fascicles at oblique angles into the internal aponeurosis (Fig. 1). In contrast, because regions of interest defined along the proximal centerline and anterior boundary of the biceps did not contain tendinous tissue, their displacements provided an accurate estimate of shortening along anterior and centerline muscle fascicles.

The different stiffness of tendon, aponeurosis, and muscle may be a principal contributor to the shortening nonuniformity measured in this study. The presence of aponeurosis tissue, which is less compliant than passive muscle tissue and more compliant than tendon (11, 16, 27, 39), could strongly influence the muscle motion during contraction. During low-load elbow flexion, only minimal stretching is expected in the distal biceps tendon; in vivo biceps brachii tendon strain has been reported as 2% during strong isometric contractions (1). However, stretching of the internal aponeurosis may occur during low-force elbow flexion because aponeurosis compliance is considerably greater than tendon compliance (11, 27, 28, 46). In addition, the compliance of muscle tissue is highly variable depending on activation state; in passive deformation studies, longitudinal muscle fiber strain was significantly larger than aponeurosis strain (39). This is consistent with our passive shortening results (Fig. 5*B*); greater shortening during elbow flexion (or alternatively, greater stretching during extension) occurs at the midportion of the muscle-tendon complex, which does not contain aponeurosis tissue.

The nonuniform centerline shortening observed in the extra-aponeurosis region raises the possibility that sarcomere length is distributed heterogeneously along individual centerline muscle fascicles. The existence of such heterogeneity has been demonstrated in preparation of single muscle fibers in animals (10, 15, 26). Sarcomere length inhomogeneity in skeletal muscle fascicles can alter the force-length property of the fascicle (47) and may be responsible for phenomena such as sarcomere popping, tension creep, and permanent extra tension (24, 29). In the human biceps brachii, the compliance of the internal aponeurosis may play a role in creating nonuniform shortening and sarcomere length heterogeneity along centerline fascicles, with additional sarcomere shortening occurring proximally at the expense of aponeurosis elongation (25). Aponeurosis elongation may also help explain the increased centerline fascicle shortening observed proximal to the aponeurosis for the higher force, 15% MVC loading condition compared with the 5% MVC loading condition (Fig. 5*B*).

The significant differences between anterior and centerline shortening measured in this study suggest that fascicle length and mean sarcomere length are not uniform throughout the biceps brachii during active elbow flexion. Even if fascicle length and mean sarcomere length were initially homogeneous within the biceps brachii, length heterogeneity would develop during elbow flexion as a result of the nonuniform shortening observed in this study. In some mammalian muscles, mean sarcomere length has been shown to be systematically and heterogeneously distributed within motor units and whole muscles (2, 20, 43). Regional variations in sarcomere length have also been found in human muscle (19, 41). Finite element analyses predict that a distribution of fiber and sarcomere lengths will develop in initially homogeneous skeletal muscles because of interactions between muscle fibers and between fibers and elastic tissue elements (35, 40). For example, it has been shown that aponeurosis compliance (3, 46) and curving of fibers and aponeuroses (35, 42, 48) can introduce heterogeneity in fascicle length and fascicle mean sarcomere length (20, 40).

Because of the limited range of the imaging coil, cine PC data were not available over the entire length of the biceps brachii. For the 12 subjects in this study, the internal aponeurosis spanned the distal 34 ± 4% of L_M, suggesting a centerline fascicle length of 66% L_M. Our results are similar to those of a cadaver study that reported mean optimal fascicle length and mean optimal L_M as 12.8 ± 3.2 and 21.6 ± 4.5 cm, respectively (33); normalized muscle fascicle length was 59% L_M (= 12.8 cm/21.6 cm), which implies a normalized aponeurosis length of 41% L_M. In the biceps brachii, muscle fascicles are staggered in a distal-to-proximal direction, with anterior fascicles inserting distally and centerline fascicles inserting proximally into the internal aponeurosis (Fig. 1). Assuming uniform optimal fascicle length, our results suggest anterior fascicles span the distal 66% of L_M. Similarly, centerline fascicles insert into the proximal end of the internal aponeurosis, at 34% L_M, and span the proximal 66% of the muscle. We report shortening over the distal 70% of L_M, which suggests our data span the entire length of anterior fascicles but only the distal half of centerline fascicles. To confirm that mean fascicle shortening differs significantly among anterior and centerline fascicles, shortening must be measured along the entire length of the biceps brachii.

The significant differences between anterior and extra-aponeurosis centerline shortening imply that sarcomere lengths differ between anterior and centerline fascicles. If these differences persist over the unmeasured proximal third of the biceps brachii, then mean sarcomere length would also differ among fascicles. Heterogeneity in mean sarcomere length among fascicles has important implications for the mechanical properties and function of skeletal muscle. A distribution of mean sarcomere length suggests fascicles likely achieve their optimal lengths at different overall muscle lengths. This would broaden the force-length curve of a muscle (12), enhancing the length range of active force generation at the expense of maximum force-generating capability at optimum muscle length (20, 43). It has been hypothesized that this "staggering" of

fascicle force-length curves with respect to muscle length may be responsible for the larger-than-expected potential length range of force production of the human rectus femoris (18) and rat semimembranosus muscles (23).

Most lumped-parameter models of muscle-tendon contraction mechanics assume that muscle fascicles shorten uniformly along their length and that whole muscles behave essentially like scaled sarcomeres (22, 44). However, this commonly used biomechanical modeling assumption may be inappropriate for many muscles because of their complex muscle-tendon architectures (17). Discrepancies have been observed between actual experimental data and the prediction of muscle function based on models that assume uniform contraction (3, 4). Our results suggest that it may be unrealistic to consider the biceps brachii as a uniformly contracting, lumped sarcomere and underscore the importance of including the effects of heterogeneity in models of muscle mechanics (22).

We are grateful to Norbert Pelc, Douglas Schwandt, Frances Sheehan, and Yudong Zhu for help with this work.

This work was supported by the Department of Veterans Affairs, a Stanford-National Institutes of Health (NIH) Biotechnology Training Grant, a Whitaker Foundation Graduate Fellowship, NIH Grants R01 HD-31493 and R01 HD-38962, and NIH Research Resource Grant P41 RR-09784.

REFERENCES

1. **Amis A, Prochazka A, Short D, Trend PS, and Ward A.** Relative displacements in muscle and tendon during human arm movements. *J Physiol* 389: 37–44, 1987.
2. **Bagust J, Knott S, Lewis DM, Luck JC, and Westerman RA.** Isometric contractions of motor units in a fast twitch muscle of the cat. *J Physiol* 231: 87–104, 1973.
3. **Bobbert MF, Ettema GC, and Huijing PA.** The force-length relationship of a muscle-tendon complex: experimental results and model calculations. *Eur J Appl Physiol* 61: 323–329, 1990.
4. **Bobbert MF and van Ingen Schenau GJ.** Isokinetic plantar flexion: experimental results and model calculations. *J Biomech* 23: 105–119, 1990.
5. **Brand PW, Beach RB, and Thompson DE.** Relative tension and potential excursion of muscles in the forearm and hand. *J Hand Surg [Am]* 6: 209–219, 1981.
6. **Buchanan TS, Rovai GP, and Rymer WZ.** Strategies for muscle activation during isometric torque generation at the human elbow. *J Neurophysiol* 62: 1201–1212, 1989.
7. **Drace JE and Pelc NJ.** Elastic deformation in tendons and myotendinous tissue: measurement by phase-contrast MR imaging. *Radiology* 191: 835–839, 1994.
8. **Drace JE and Pelc NJ.** Measurement of skeletal muscle motion in vivo with phase-contrast MR imaging. *J Magn Reson Imaging* 4: 157–163, 1994.
9. **Drace JE and Pelc NJ.** Tracking the motion of skeletal muscle with velocity-encoded MR imaging. *J Magn Reson Imaging* 4: 773–778, 1994.
10. **Edman KA and Reggiani C.** Redistribution of sarcomere length during isometric contraction of frog muscle fibres and its relation to tension creep. *J Physiol* 351: 169–198, 1984.
11. **Ettema GJ and Huijing PA.** Properties of the tendinous structures and series elastic component of EDL muscle-tendon complex of the rat. *J Biomech* 22: 1209–1215, 1989.
12. **Ettema GJ and Huijing PA.** Effects of distribution of muscle fiber length on active length-force characteristics of rat gastrocnemius medialis. *Anat Rec* 239: 414–420, 1994.
13. **Fukunaga T, Ichinose Y, Ito M, Kawakami Y, and Fukashiro S.** Determination of fascicle length and pennation in a contracting human muscle in vivo. *J Appl Physiol* 82: 354–358, 1997.
14. **Garland SJ, Enoka RM, Serrano LP, and Robinson GA.** Behavior of motor units in human biceps brachii during a submaximal fatiguing contraction. *J Appl Physiol* 76: 2411–2419, 1994.
15. **Gordon A, Huxley AF, and Julian F.** Tension development in highly stretched vertebrate muscle fibers. *J Physiol* 184: 143–169, 1966.
16. **Gosline JM.** Tensile materials. In: *Mechanical Design in Organisms*, edited by Wainwright SA, Biggs JD, Currey JD, and Gosline JM. New York: Wiley, 1976, p. 64–109.
17. **Herring SW, Grimm AF, and Grimm BR.** Functional heterogeneity in a multipinnate muscle. *Am J Anat* 154: 563–576, 1979.
18. **Herzog W and ter Keurs HE.** Force-length relation of in-vivo human rectus femoris muscles. *Pflügers Arch* 411: 642–647, 1988.
19. **Huijing PA.** Architecture of the human gastrocnemius muscle and some functional consequences. *Acta Anat (Basel)* 123: 101–107, 1985.
20. **Huijing PA.** Parameter interdependence and success of skeletal muscle modelling. *Hum Mov Sci* 14: 443–486, 1995.
21. **Huijing PA.** Muscle as a collagen fiber reinforced composite: a review of force transmission in muscle and whole limb. *J Biomech* 32: 329–345, 1999.
22. **Huijing PA.** Modeling of homogeneous muscle: is it realistic to consider skeletal muscle as a lumped sarcomere or fiber? In: *Biomechanics and Neural Control of Posture and Movement*, edited by Winters JM and Crago PE. New York: Springer, 2000, p. 92–98.
23. **Huijing PA, van Lookeren Campagne AA, and Koper JF.** Muscle architecture and fibre characteristics of rat gastrocnemius and semimembranosus muscles during isometric contractions. *Acta Anat (Basel)* 135: 46–52, 1989.
24. **Julian FJ and Morgan DL.** Intersarcomere dynamics during fixed-end tetanic contractions of frog muscle fibres. *J Physiol* 293: 365–378, 1979.
25. **Kawakami Y and Lieber RL.** Interaction between series compliance and sarcomere kinetics determines internal sarcomere shortening during fixed-end contraction. *J Biomech* 33: 1249–1255, 2000.
26. **Lieber RL and Baskin RJ.** Intersarcomere dynamics of single muscle fibers during fixed-end tetani. *J Gen Physiol* 82: 347–364, 1983.
27. **Lieber RL, Leonard ME, Brown CG, and Trestik CL.** Frog semitendinosis tendon load-strain and stress-strain properties during passive loading. *Am J Physiol Cell Physiol* 261: C86–C92, 1991.
28. **Maganaris CN and Paul JP.** Load-elongation characteristics of in vivo human tendon and aponeurosis. *J Exp Biol* 203: 751–756, 2000.
29. **McMahon TA.** *Muscles, Reflexes, and Locomotion.* Princeton, NJ: Princeton Univ. Press, 1984.
30. **Miller KJ, Garland SJ, Ivanova T, and Ohtsuki T.** Motor-unit behavior in humans during fatiguing arm movements. *J Neurophysiol* 75: 1629–1636, 1996.
31. **Monti RJ, Roy RR, Hodgson JA, and Edgerton VR.** Transmission of forces within mammalian skeletal muscles. *J Biomech* 32: 371–380, 1999.
32. **Morgan DL.** From sarcomeres to whole muscles. *J Exp Biol* 115: 69–78, 1985.
33. **Murray WM, Buchanan TS, and Delp SL.** The isometric functional capacity of muscles that cross the elbow. *J Biomech* 33: 943–952, 2000.
34. **Narici M.** Human skeletal muscle architecture studied in vivo by non-invasive imaging techniques: functional significance and applications. *J Electromyogr Kinesiol* 9: 97–103, 1999.
35. **Otten E.** Concepts and models of functional architecture in skeletal muscle. *Exerc Sport Sci Rev* 16: 89–137, 1988.
36. **Pappas G.** *Characterization of Biceps Brachii Architecture and Contraction Mechanics Using Medical Imaging Techniques* (PhD dissertation). Stanford, CA: Stanford Univ., 2001.

37. **Pelc NJ, Herfkens RJ, Shimakawa A, and Enzmann DR.** Phase contrast cine magnetic resonance imaging. *Magn Reson Q* 7: 229–254, 1991.
38. **Sheehan FT, Zajac FE, and Drace JE.** Using cine phase contrast magnetic resonance imaging to non-invasively study in vivo knee dynamics. *J Biomech* 31: 21–26, 1998.
39. **Van Bavel H, Drost MR, Wielders JD, Huyghe JM, Huson A, and Janssen JD.** Strain distribution on rat medial gastrocnemius (MG) during passive stretch. *J Biomech* 29: 1069–1074, 1996.
40. **Van der Linden BJ, Koopman HF, Grootenboer HJ, and Huijing PA.** Modelling functional effects of muscle geometry. *J Electromyogr Kinesiol* 8: 101–109, 1998.
41. **Van Eijden TM and Raadsheer MC.** Heterogeneity of fiber and sarcomere length in the human masseter muscle. *Anat Rec* 232: 78–84, 1992.
42. **Van Leeuwen JL and Spoor CW.** Modelling the pressure and force equilibrium in unipennate muscles with in-line tendons. *Philos Trans R Soc Lond B Biol Sci* 342: 321–333, 1993.
43. **Willems ME and Huijing PA.** Heterogeneity of mean sarcomere length in different fibres: effects on length range of active force production in rat muscle. *Eur J Appl Physiol* 68: 489–496, 1994.
44. **Zajac FE.** Muscle and tendon: properties, models, scaling, and application to biomechanics and motor control. *Crit Rev Biomed Eng* 17: 359–411, 1989.
45. **Zhu Y, Drangova M, and Pelc NJ.** Fourier tracking of myocardial motion using cine-PC data. *Magn Reson Med* 35: 471–480, 1996.
46. **Zuurbier CJ, Everard AJ, van der Wees P, and Huijing PA.** Length-force characteristics of the aponeurosis in the passive and active muscle condition and in the isolated condition. *J Biomech* 27: 445–453, 1994.
47. **Zuurbier CJ, Heslinga JW, Lee-de Groot MB, and Van der Laarse WJ.** Mean sarcomere length-force relationship of rat muscle fibre bundles. *J Biomech* 28: 83–87, 1995.
48. **Zuurbier CJ and Huijing PA.** Changes in geometry of actively shortening unipennate rat gastrocnemius muscle. *J Morphol* 218: 167–180, 1993.